



1 **The Response of the Amazon Ecosystem to the Photosynthetically Active**
2 **Radiation Fields: Integrating Impacts of Biomass Burning Aerosol and**
3 **Clouds in the NASA GEOS ESM**

4
5 Huisheng Bian^{1,2}, Eunjee Lee^{3,4}, Randal D. Koster⁴, Donifan Barahona⁴, Mian Chin², Peter R.
6 Colarco², Anton Darmenov², Sarith Mahanama^{5,4}, Michael Manyin^{5,4}, Peter Norris^{3,4}, John
7 Shilling⁶, Hongbin Yu², and Fanwei Zeng^{5,4}

8
9 ¹Joint Center for Environmental Technology UMBC, Baltimore, MD, 21250, USA

10 ²Laboratory for Atmospheres, NASA Goddard Space Flight Center, Greenbelt, MD, 20771, USA

11 ³Goddard Earth Sciences Technology and Research, Universities Space Research Association,
12 Columbia, MD 21046, USA

13 ⁴Global Modeling and Assimilation Office, NASA Goddard Space Flight Center, Greenbelt, MD
14 20771, USA

15 ⁵Science Systems and Applications, Inc., Lanham, MD 20706, USA

16 ⁶Atmospheric Sciences & Global Change Division, Pacific Northwest National Laboratory,
17 Richland, WA 99352, USA

18
19 *Correspondence to:* Huisheng Bian (Huisheng.Bian@nasa.gov)

20
21 **Abstract**

22
23 The Amazon experiences fires every year, and the resulting biomass burning aerosols, together
24 with cloud particles, influence the penetration of sunlight through the atmosphere, increasing the
25 ratio of diffuse to direct photosynthetically active radiation (PAR) reaching the vegetation
26 canopy and thereby potentially increasing ecosystem productivity. In this study, we use the
27 NASA Goddard Earth Observing System (GEOS) model running with coupled aerosol, cloud,
28 radiation, and ecosystem modules to investigate the impact of Amazon biomass burning aerosols
29 on ecosystem productivity, as well as the role of the Amazon's clouds in tempering the impact.
30 The study focuses on a seven-year period (2010-2016) during which the Amazon experienced a
31 variety of dynamic environments (e.g., La Niña, normal years, and El Niño). The radiative
32 impacts of biomass burning aerosols on ecosystem productivity—call here the aerosol light
33 fertilizer effect—are found to increase Amazonian Gross Primary Production (GPP) by 2.6% via
34 a 3.8% increase in diffuse PAR (DFPAR) despite a 5.4% decrease in direct PAR (DRPAR) on
35 multiyear average. On a monthly basis, this increase in GPP can be as large as 9.9% (occurring
36 in August 2010). Consequently, the net primary production (NPP) in the Amazon is increased by
37 1.5%, or $\sim 92 \text{ TgCyr}^{-1}$ —equivalent to $\sim 37\%$ of the carbon lost due to Amazon fires over the seven
38 years considered. Clouds, however, strongly regulate the effectiveness of the aerosol light
39 fertilizer effect. The efficiency of the fertilizer effect is highest for cloud-free conditions and
40 linearly decreases with increasing cloud amount until the cloud fraction reaches ~ 0.8 , at which
41 point the aerosol-influenced light changes from being a stimulator to an inhibitor of plant
42 growth. Nevertheless, interannual changes in the overall strength of the aerosol light fertilizer
43 effect are primarily controlled by the large interannual changes in biomass burning aerosols
44 rather than by changes in cloudiness during the studied period.

45
46



47 1. Introduction

48 The Amazon is home to more than 34 million people and hosts a large variety of plants and
49 animals. The rainforest plays a vital role in the global climate, regulating temperatures and
50 storing vast quantities of carbon dioxide (Laurance 1999; Nepstad et al., 2008). It is matter of
51 intense research whether light or water is the limiting factor that controls plant growth over
52 Amazonia. Considerable evidence demonstrates that sunlight indeed drives Amazon forest
53 growth (Doughty et al., 2019; Huete et al., 2006; Myneni et al., 2007) although water deficit
54 could be a limiting factor during severe droughts (Doughty et al., 2015; Feldpausch et al., 2016;
55 Saatchi et al., 2013). Satellite observations show a clear seasonal cycle with a gradual crescendo
56 in both leaf area and incoming surface sunlight beginning at the onset of the dry season (~August
57 – November) (Myneni et al., 2007). Vegetation index maps also show that a majority of
58 Amazonia is greener in the dry season than in the wet season (~mid-December – mid-May)
59 (Huete et al., 2006). It is in the dry season, when light becomes a key-controlling factor for forest
60 productivity, that the Amazon forest thrives.

61
62 Plant photosynthesis requires sunlight to reach the leaves of the canopy. While aerosols and
63 clouds in the atmosphere decrease the total amount of light that reaches the canopy, they also
64 increase scattering, thereby increasing the ratio of diffuse radiation to direct radiation. This is
65 important because the efficiency of plant photosynthesis increases under diffuse sunlight – a
66 phenomenon both explained theoretically (Rap et al., 2015; Roderick et al., 2001; Zhou et al.,
67 2020) and observed in the field (Cirino et al., 2014; Doughty et al., 2010; Ezhova et al., 2018; Gu
68 et al., 2003; Lee et al., 2018; Niyogi et al., 2004; Oliveira et al., 2007). Leaf photosynthesis
69 increases nonlinearly with solar radiation, becoming saturated on bright days at light levels
70 above which leaves cannot take more light (Gu et al., 2003; Mercado et al., 2009). Under clear
71 and clean sky conditions, particularly around midday, sunlight is mainly direct, and while this
72 allows the sunlit leaves on top to be light saturated, the shaded leaves below them receive
73 relatively little sunlight and thus participate less in photosynthesis (Rap et al., 2015; Roderick et
74 al., 2001). In contrast, under cloudy conditions or in the presence of aerosols, much of the
75 midday light is diffuse, and diffuse light can penetrate deeper into the canopy and illuminate
76 shaded leaves. Li and Yang (2015) conducted a chamber experiment to explore diffuse light on
77 light distribution within a canopy and the resulting effects on crop photosynthesis and plant
78 growth. They concluded that diffusion of the incident light improves spatial light distribution,
79 lessens the variation of temporal light distribution in the canopy, and allows more light-
80 stimulated growth of shade-tolerant potted plants.

81
82 The situation is more profound during the Amazon dry season when intensive seasonal fires
83 release large amounts of primary aerosol particles as well as gas precursors that form secondary
84 organic and inorganic aerosols. Using stand-alone radiation and vegetation models, Rap et al.
85 (2015) concluded that fires over the Amazon dry season increase Amazon net primary
86 production (NPP) by 1.4–2.8% by increasing diffuse radiation. This enhancement of Amazon
87 basin NPP (78–156 Tg C a⁻¹) is equivalent to 33–65% of the annual regional carbon emissions
88 from biomass burning and accounts for 8–16% of the observed carbon sink across mature
89 Amazonian forests. Moreira et al. (2017) advanced this analysis by coupling an ecosystem
90 module and aerosol model within a Eulerian transport model. Their study indicated that biomass
91 burning aerosols lead to increases of about 27% in Amazonian Gross Primary Production (GPP)
92 and 10% in plant respiration as well as a decline in soil respiration of 3 %. However, their



93 approach assumes cloud-free conditions through their use of a diffuse irradiance
94 parameterization based on the multiwavelength aerosol optical depth (AOD) measurement.
95 Malavelle et al. (2019) explored the overall net impact of biomass burning aerosol on the
96 Amazon ecosystem using an Earth System Model (ESM) (HadGEM2-ES). They estimated NPP
97 to increase by +80 to +105 TgC yr⁻¹, or 1.9% to 2.7%, ascribing this net change to an increase in
98 diffuse light, a reduction in the total amount of radiation, and feedback from climate adjustments
99 in response to the aerosol forcing. Their study takes into account the dynamic feedback of short
100 lifetime cloud fields. However, it does not address the role of Amazon background clouds and
101 their interannual changes on the aerosol-ecosystem impact.
102

103 When clouds and aerosol co-exist, the impact from clouds on the ecosystem typically dominates
104 because clouds are optically thicker. The surface sunlight for cloudy versus cloud-free conditions
105 can differ greatly even if the AOD is the same. (Note that, unless specified otherwise, solar
106 radiation in this study refers to the wavelength range of 400-700 nm, i.e., photosynthetically
107 active radiation, or PAR). Measurements indicate that the desirable range of clearness index (CI)
108 -- the fraction of incoming total sunlight that reaches the canopy -- is around 0.4-0.7 for some
109 forest ecosystems and above 0.3 for peatland (Butt et al., 2010, Letts and Lafleur, 2005). Quite
110 often a low CI occurs during a cloudy day, but on occasion it might result from the presence of a
111 very thick aerosol layer. As suggested above, if CI is high, the diffuse fraction of the total solar
112 radiation is low, and the overall productivity of the canopy is reduced. For example, Cirino et al.
113 (2014) found that the net ecosystem exchange (NEE) of CO₂ is increased by 29% and 20% in
114 two Amazon stations (the Jaru Biological Reserve (RBJ) and the Cuieiras Biological Reserve at
115 the K34 Large-Scale Biosphere-Atmosphere Experiment in Amazonia (LBA) tower),
116 respectively, when AOD is 0.1-1.5 at 550nm under clear conditions. Higher AOD (> 3) leads to a
117 strong reduction in photosynthesis (via reducing PAR) up to the point where NEE approaches
118 zero. Oliveira et al. (2007) found that Amazon forest productivity was enhanced under
119 moderately thick smoke loading because of an increase of diffuse solar radiation, but large
120 aerosol loading (i.e., AOD > 2.7) results in lower net productivity of the Amazon forest.
121

122 Despite its name, the Amazon's "dry season" (June-November) still features significant
123 cloudiness, and the interannual variations in the clouds can be large. Furthermore, rain does fall
124 during the dry season – close to 40% of the total annual precipitation falls therein. Clouds in the
125 dry season are mostly formed by small-scale processes that influence the weather (see an
126 example of a uniform layer of "popcorn" clouds observed by Moderate Resolution Imaging
127 Spectroradiometer (MODIS) on 08/19/2009 in
128 <http://earthobservatory.nasa.gov/IOTD/view.php?id=39936>). It is during this period, when
129 sunlight (particularly diffuse light) drenches the trees due to reduced rain (and fewer clouds)
130 relative to the wet season, that the forest grows the most. Consideration of the joint effects of
131 clouds and biomass burning aerosols on diffuse and direct PAR during the dry season is thus
132 particularly important.
133

134 This study has two objectives. First, we investigate how Amazon biomass burning aerosols
135 (BBAer) affect the land productivity (i.e., GPP and NPP) via their impact on direct and diffuse
136 PAR (DRPAR and DFPAR). Second, we investigate the sensitivity of the BBAer light fertilizer
137 effect to the presence of the Amazon dry season cloud fields within the range indicated by the
138 potential interannual variation of the clouds. We use in our analysis a version of the NASA



139 GEOS ESM that includes coupling between aerosol, cloud, radiation, and ecosystem processes.
140 To our knowledge, only one other study has used an ESM to investigate such fire impacts across
141 Amazonia (Malavelle et al., 2019), and as noted above, this study did not address the ability of
142 Amazon clouds to temper the BBAer impacts. Accordingly, our study is the first ESM-based
143 study to investigate the BBAer light fertilizer effect within a range of interannual Amazon cloud
144 levels. Together our objectives provide a full and comprehensive study of BBAer light fertilizer
145 effect in a context of potential Amazon dry season atmospheric conditions.

146

147 It is necessary to point out, however, that our study focuses only on the impact of Amazon
148 biomass burning aerosol. We do not consider the radiative impacts of other potentially important
149 aerosols. These other aerosol types have been examined in various observational studies (e.g.,
150 Cirino et al., 2014; Ezhova et al., 2018; Hemes et al., 2020; Wang et al., 2018, Yan et al., 2014)
151 and model investigations that focus, for example, on anthropogenic aerosol (Keppel et al., 2016);
152 O'Sullivan et al., 2016), dust (Xi et al., 2012), biogenic aerosol (Rap et al., 2018; Sporre et al.,
153 2019), volcanic aerosol (Gu et al., 2003), and the general aerosol field (Feng et al., 2019).

154

155 The paper is organized as follows. Section 2 describes the NASA GEOS ESM and its relevant
156 modules (section 2.1), the observational data used for model evaluation and explanation (section
157 2.2), and the experimental setup (section 2.3). Section 3 provides an evaluation of the model
158 (section 3.1), basic theory regarding the impact of aerosol and cloud on the surface downward
159 radiation (section 3.2), results regarding the simulated ecosystem response to BBAer-induced
160 radiation changes (section 3.3), and the impacts of Amazon background clouds on this response
161 (section 3.4). A final summary is provided in section 4.

162

163 **2. Model description, data application, and experiment setup**

164

165 **2.1 Model description**

166 The GEOS modeling system connects state-of-the-art models of the various components of the
167 Earth's climate system together using the Earth System Modeling Framework (ESMF) (Molod et al.,
168 2015; 2012; Rienecker et al., 2011; <https://gmao.gsfc.nasa.gov/>). We discuss here the
169 components of the system that are particularly relevant to our study, including aerosol, cloud
170 microphysics, radiative transfer, and land ecosystem modules.

171

172 GEOS Goddard Chemistry Aerosol Radiation and Transport (GOCART) simulates a number of
173 major atmospheric aerosol species and precursor gases from natural and anthropogenic sources,
174 including sulfate, nitrate, ammonium, black carbon (BC), organic aerosol (OA, including
175 primary and secondary OA), dust, sea salt, dimethyl sulfide (DMS), SO₂, and NH₃ (Bian et al.,
176 2010, 2013, 2017, 2019; Chin et al., 2009, 2014; Colarco et al., 2010, 2017; Murphy et al., 2019;
177 Randles et al., 2013). Monthly emissions from shipping, aircraft, and other anthropogenic
178 sources are obtained from the recent CMIP6 CEDS emission inventory. Daily biomass burning
179 emissions are provided by GFED4s

180 (https://daac.ornl.gov/VEGETATION/guides/fire_emissions_v4.html). Estimates of degassing
181 and eruptive volcanic emissions are derived from Ozone Monitoring Instrument (OMI) satellite
182 (Carn et al., 2017). Emissions of dust, sea salt, and DMS are dynamically calculated online as a
183 function of the model-simulated near-surface winds and other surface properties. A more recent
184 augmentation of GOCART relevant to this study involves the modification of the absorbing



185 properties of “brown carbon” (Colarco et al., 2017). The simulation of primary organic carbon
186 (POA) and secondary organic carbon (SOA) is particularly important for this study. Previous
187 versions of GOCART in GEOS were simple regarding SOA productions, relating biogenic SOA
188 to a prescribed “climatological” monthly terpene emission – SOA production was assumed to be
189 10% of terpene emission (i.e., SOA yield of 10%). The new version calculates the emission of
190 VOCs online as a function of light and temperature using the Model of Emissions of Gases and
191 Aerosols from Nature (MEGAN) version 2.1 (Guenther et al., 2012). The biogenic SOA is then
192 derived by applying an SOA yield of 3% to isoprene and 5% to monoterpene following the
193 suggestion of Kim et al. (2015). This newer version of GOCART also introduces a
194 parameterization of SOA from anthropogenic and biomass burning sources based on Hodzic et
195 al. (2011) and Kim et al. (2015).

196
197 The GEOS two-moment cloud microphysics module is used in this study. The module includes
198 the implementation of a comprehensive stratiform microphysics module, a new cloud coverage
199 scheme that allows ice supersaturation, and a new microphysics module embedded within the
200 moist convection parameterization (Barahona et al., 2014). At present, aerosol number
201 concentrations are derived from the GEOS/GOCART-calculated aerosol mass mixing ratio and
202 prescribed size distributions and mixing state, which are then used for cloud condensation nuclei
203 (CCN) activation (following the approach of Abdul-Razzak and Ghan, 2000) and ice nucleation
204 (following the approach of Barahona and Nenes, 2009) processes. Aerosol-cloud interactions are
205 thus accounted for in our simulation. The model calculates various cloud properties, including
206 cloud fraction, cloud droplet and ice crystal number concentrations and effective radii, and cloud
207 liquid and ice water paths. These fields have been evaluated against satellite observations and
208 field measurements; the model shows a realistic simulation of cloud characteristics despite a few
209 remaining deficiencies (Barahona et al., 2014, Breen et al., 2020).

210
211 The current default GEOS solar radiation transfer module is the shortwave rapid radiation
212 transfer model for GCMs (RRTMG_SW), a correlated k-distribution model (Iacono et al., 2008).
213 This GCM version utilizes a reduced complement of 112 g-points, which is half of the 224 g-
214 points used in the standard RRTMG_SW, and a two-stream method for radiative transfer. Total
215 fluxes are accurate to within 1-2 W/m² relative to the standard RRTMG_SW (using DISORT)
216 with aerosols in clear sky and within 6 W/m² in overcast sky. RRTMG_SW with DISORT is
217 itself accurate to within 2 W/m² of the data-validated multiple scattering model, CHARTS.
218 RRTMG_SW specifically calculates the direct and diffuse components of PAR (400-700 nm)
219 separately. The GEOS atmospheric radiative transfer calculation is designed in a way that allows
220 users to examine the impact of various combinations of atmospheric aerosol and cloud fields on
221 radiation. In addition to the standard calculation of solar radiation for ambient atmospheric
222 conditions, diagnostic calculations can be carried out by repeating the calculation of the radiation
223 transfer scheme with different combinations of atmospheric conditions: clean air (no aerosols),
224 clear air (no clouds), and clean plus clear air. Using this architecture, for this study we modify
225 the radiation scheme to allow the additional diagnosis of radiation fields under conditions of zero
226 BB-aerosols but retained non-BB-aerosols and ambient clouds.

227
228 The catchment land surface model (LSM) with carbon and nitrogen physics (Catchment-CN) in
229 GEOS is in essence a merger of the C-N physics within the NCAR–DOE Community Land
230 Model (CLM) (Oleson et al. 2010, 2013; Lawrence et al., 2019) version 4.0 and the energy and



231 water balance calculations of the NASA GMAO catchment LSM (Koster et al. 2000). The
232 original NASA catchment LSM used a prescribed representation of phenology (leaf area index,
233 or LAI, and greenness fraction) to compute the canopy conductance, the parameter describing
234 the ease with which the plants transpire water. In Catchment-CN, photosynthesis and
235 transpiration depend non-linearly on solar radiation. The canopy is assumed to consist of sunlit
236 leaves and shaded leaves, and the DRPAR and DFPAR absorbed by the vegetation is
237 apportioned to the sunlit and shaded leaves as described by Thornton and Zimmermann (2007).
238 The prognostic carbon storages underlying the phenological variables are computed as a matter
239 of course along with values of canopy conductance that reflect an explicit treatment of
240 photosynthesis physics. These canopy conductances, along with the LAIs diagnosed from the
241 new carbon prognostic variables, are fed into the energy and water balance calculations in the
242 original catchment LSM. The output fluxes from the merged system include carbon fluxes in
243 addition to traditional fluxes of heat and moisture. The merger of the two models allows
244 Catchment-CN to follow 19 distinct vegetation types. Koster and Walker (2015) have used
245 Catchment-CN within an atmospheric global circulation model (AGCM) framework to
246 investigate interactive feedback among vegetation phenology, soil moisture, and temperature. In
247 this study, the modeled atmospheric CO₂ from the AGCM is used to drive the carbon, water, and
248 energy dynamics in the Catchment-CN model.

249 In addition to the GEOS ESM, we use a photolysis scheme, FastJX, in its stand-alone mode to
250 explore how incoming solar radiation penetrates the atmosphere in the presence of aerosols and
251 clouds in order to enhance our basic understanding of the role of atmospheric particles on
252 radiation. FastJX is based on the original Fast-J scheme, which was developed for tropospheric
253 photochemistry with interactive consideration of aerosol and cloud impacts at 291–850 nm (Wild
254 et al., 2000), and Fast-J2, which extended the scheme into the deep UV spectrum range of 177-
255 291 nm (Bian and Prather, 2002).
256

257 **2.2 Observational data**

258 We mostly rely on the GoAmazon (“Green Ocean Amazon”) field campaign
259 (<http://campaign.arm.gov/goamazon2014/>) for in situ site-level aerosol surface observations and
260 local-area vertical distribution measurements used to assess the model OA concentrations.
261 GoAmazon is an integrated field campaign conducted in the central Amazon Basin (Martin et al.,
262 2010). Specifically, we use the surface OA concentration measured in 2014 by the Aerosol
263 Chemical Speciation Monitor (ACSM) operated by the Department of Energy’s (DOE)
264 Atmospheric Radiation Measurement (ARM) Mobile Facility located 70 km downwind of
265 Manaus, Brazil (Ng et al., 2011). We also use the measurement of surface CO volume mixing
266 ratio in 2014 at Manaus by Los Gatos Research (LGR) N₂O/CO Analyzer that uses LGR’s
267 patented Off-axis Integrated Cavity Output Spectroscopy (ICOS) technology. Also used is the
268 vertical profile of OA concentration measured by a time-of-Flight Aerosol Mass Spectrometer
269 (ToF-AMS) instrument on the ARM Aerial Facility Gulfstream-1 (G-1) aircraft during the dry
270 season of 2014 (Sept 06–Oct 04, 2014) (Shilling et al., 2018). The G-1 aircraft was based out of
271 the Manaus International airport and flew patterns designed to intersect the Manaus urban plume
272 at increasing downwind distance from the city (e.g., 59–61°W and 4–2.5°S). In addition, we
273 evaluate the model with AOD and single scattering albedo (SSA) measurements taken at a
274 central Amazon station (Alta Floresta) in the ground-based Aerosol Robotic Network
275 (AERONET) sun photometer network (<http://aeronet.gsfc.nasa.gov>). We also use MODIS



276 collection 6.1 level-3 AOD product (<http://modis.gsfc.nasa.gov/data/dataproduct/index.php>), which
277 is characterized by observations with large spatial coverage.

278
279 MODIS cloud products (<https://modis-atmosphere.gsfc.nasa.gov/data/dataproduct/>), specifically
280 total cloud fraction and cloud optical depth in liquid and ice particles, were used to evaluate the
281 model cloud simulation. We use the cloud data from MODIS collection 6.1 MYD08_D3, a level-
282 3 $1^\circ \times 1^\circ$ global gridded monthly joint product derived from the MODIS level-2 pixel level
283 products. MODIS level 2 cloud fraction is produced by the infrared retrieval methods during
284 both day and night at a 5×5 1-km-pixel resolution. Level 2 cloud optical thickness used in this
285 study is derived using the MODIS visible and near-infrared channel radiances from the Aqua
286 platform.

287
288 The satellite-derived Clouds and the Earth's Radiant Energy System product CERES-EBAF was
289 used to evaluate the GEOS simulation of radiation fields. CERES-EBAF retrieves surface
290 downward shortwave radiation (R_{SFC}) using cloud information from more recent satellite data
291 (MODIS, CERES, CloudSat and CALIPSO) and aerosol fields from AERONET/MODIS
292 validation-based estimates (Kato et al., 2013). This global product is provided at a $1^\circ \times 1^\circ$
293 horizontal resolution and covers the years 2000-2015 for both all- and clear-sky conditions. The
294 multiyear R_{SFC} products provide both a regional and a time evolution view of radiation over
295 Amazonia.

296 Two observations-based GPP products were used to evaluate the GEOS ecosystem simulations.
297 Through upscaling using machine learning methods (Jung et al., 2020), the FluxCom GPP
298 product provides globally distributed eddy-covariance-based estimates of carbon fluxes between
299 the biosphere and the atmosphere. FluxSat GPP is estimated with models that use satellite data
300 (e.g., MODIS reflectances and solar-induced fluorescence (SIF)) within a simplified light-use
301 efficiency framework (Joiner et al., 2018). We used monthly GPP for August through October of
302 2010-2015 in this study.

303 2.3 Experiment setup

304 All experiments were run with the coupled atmosphere and land components of the NASA
305 GEOS ESM system discussed above. The sea surface temperature (SST) for the atmospheric
306 dynamic circulation is provided by the GEOS Atmospheric Data Assimilation System (ADAS)
307 that incorporates satellite and in situ SST observations and assimilates Advanced Very High
308 Resolution Radiometer (AVHRR) brightness temperatures. The experiments were run in replay
309 mode, which means that the model dynamical variables (winds, pressure, temperature, and
310 humidity) were set, every 6 hours, to the values archived by the Modern-Era Retrospective
311 Analysis for Research and Applications version 2 (MERRA-2) meteorological reanalysis (Gelaro
312 et al. 2017); a 6-hourly forecast provided the dynamical and physical fields between the 6-hour
313 resets. In effect, the replay approach forces the atmospheric “weather” simulated in the model to
314 agree with the reanalysis. All designed experiments were run over 2010-2016, a period that
315 includes La Niña (2010-2011), El Niño (2015-2016), and neutral years as indicated by the
316 Oceanic Niño Index (ONI, <https://origin.cpc.ncep.noaa.gov/>).

317
318 Our experimental design makes extensive use of GEOS's highly flexible configuration. First, the
319 GEOS GOCART module includes a tagged aerosol mechanism. Each specific aerosol



320 component in GOCART is simulated independently from the others, and the contribution of each
 321 emission type to the total aerosol mass is also not interfered by that of other emission types.
 322 Thus, additional aerosol tracers can easily be “tagged” according to emission source types. This
 323 makes it possible for GOCART to calculate and transfer two sets of aerosol fields (e.g., one with
 324 and one without a biomass burning source) to the radiation module. Second, the radiation module
 325 can in turn calculate a set of atmospheric radiation fields corresponding to each set of aerosol
 326 fields, and it can then disseminate both sets of radiation fields to the various components of
 327 interest (i.e., cloud module, land ecosystem module, etc.) according to the needs of our
 328 experiments (see below).
 329

330 Table 1 provides a brief summary of the experiments performed for this study. First, we designed
 331 a pair of experiments (allaer and nobbaer, hereafter referred to as “pair1”) to explore the BBAer
 332 light fertilizer effect on the land productivity via PAR (objective 1). The allaer and nobbaer
 333 experiments are designed to simulate the same atmospheric dynamics but send different PAR
 334 fluxes into the Catchment-CN model. Specifically, both the allaer and nobbaer experiments used
 335 all atmospheric aerosols including real-time biomass burning emissions over 2010-2016 to
 336 calculate a set of radiation fields (R^1) to drive atmospheric circulation; however, with the help of
 337 GEOS’s flexible configuration, the nobbaer experiment also calculated a second set of radiation
 338 fields (R^2) that used non-BB aerosols only. R^1 was sent to Catchment-CN in the allaer
 339 experiment whereas R^2 was sent to Catchment_CN in the nobbaer experiment. In this way, the
 340 only difference between the allaer and nobbaer experiments was the PAR fluxes used to drive the
 341 ecosystem model – only the PAR fluxes used in allaer reflected the presence of biomass burning
 342 aerosols. The atmospheric meteorological fields in the two experiments, including clouds, skin
 343 temperature, and soil moisture, show only minor differences stemming from land feedback
 344 (Figure S1-2, Table S1e and Table S2e).
 345

346 Table 1. Designed experiments (2010-2016) with their perturbation on aerosol fields and
 347 subsequent impact on radiation and ecosystem

Exp Name	Aerosol	R in RRTMG	R driving circulation	R driving Catchment-CN	Purpose
Pair 1	allaer	Standard all, w/ Realltime AERbb emission	$R^1_{top}, R^1_{dir}, R^1_{diff}$ (all aerosol)	R^1_{dir}, R^1_{diff}	Check atmospheric BB aerosol impact on plants via radiation fields during 2010-2016
	nobbaer		$R^1_{top}, R^1_{dir}, R^1_{diff}$ (all aerosol) $R^2_{top}, R^2_{dir}, R^2_{diff}$ (all non-bb aerosol)	R^2_{dir}, R^2_{diff}	
Pair 2	callaer	Standard all, w/ AERbb emission fixed at 2010	$R^1_{top}, R^1_{dir}, R^1_{diff}$ (all aerosol)	R^1_{dir}, R^1_{diff}	Check how clouds adjust the above impact
	cnobbaer		$R^1_{top}, R^1_{dir}, R^1_{diff}$ (all aerosol) $R^2_{top}, R^2_{dir}, R^2_{diff}$ (all non-bb aerosol)	R^2_{dir}, R^2_{diff}	

348 We also designed a pair of experiments (callaer and cnobbaer, hereafter referred to as “pair2”) to
 349 address the sensitivity of the BBAer light fertilizer effect to the presence of the Amazon dry
 350 season cloud fields (objective 2). The pair2 experiments are similar to those in pair1 except that
 351 the particular BB emissions of year 2010 were repeated during all seven years. Applying a fixed
 352 aerosol emission allows us to attribute the interannual variation of the ecosystem solely to the
 353 influence of interannual variations in atmospheric metrological fields, including clouds. In
 354 addition, combining the pair1 and pair2 experiments provides two biomass burning aerosol
 355 emissions for each year except 2010, which allows us to compare the impacts of different
 356 emissions under similar meteorological environments (Figure S1-2, Table S1e and Table S2e).
 357



358 Given that the experiment period covers strong La Niña and El Niño years, we can examine
359 BBaer impacts on ecosystem productivity under the full range of Amazon background cloud
360 fields.

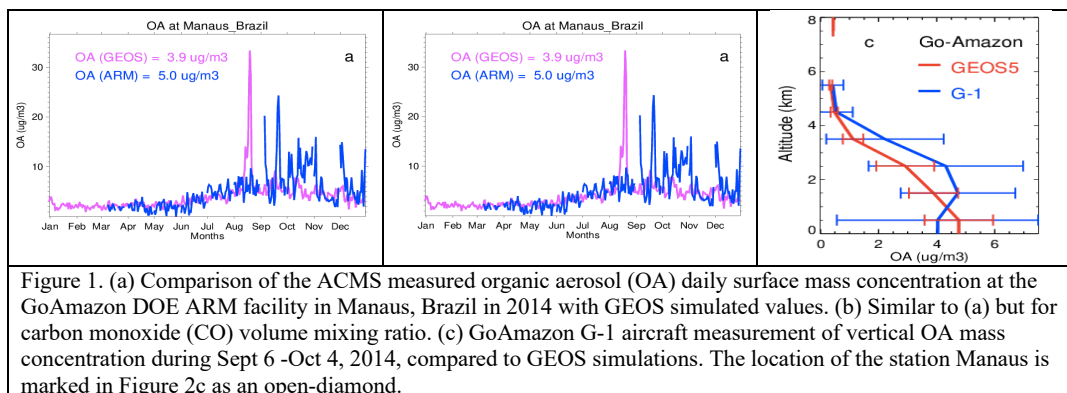
362 3. Results and Discussion

363 3.1 Evaluation of GEOS simulations of aerosol, cloud, radiation, and ecosystem 364 response

366 The NASA GEOS ESM model, including its aerosol, cloud, radiation, and ecosystem modules as
367 used in the baseline simulation (i.e., experiment allaer), has been evaluated extensively and
368 utilized in a number of scientific studies. However, a majority of the aerosol studies have
369 focused on the simulation of aerosols over the Northern Hemisphere. Past studies with GEOS
370 have not provided a detailed model evaluation over South America during our study period. We
371 provide such an evaluation here.

372
373 The simulated tracer fields are compared with measurements over the Amazon in Figures 1 and
374 2. Figure 1 shows results for surface OA concentration, surface CO concentration, and the OA
375 concentration vertical profile. We focus primarily on the OA evaluation since we are interested
376 in biomass burning aerosols from fires. Figure 1a shows the comparison of surface daily OA
377 concentration between the model simulation and the GoAmazon measurements at Manaus,
378 Brazil, in 2014 (The location is indicated in Figure 2c with an open-diamond). The simulated OA
379 broadly captures the seasonal trend in OA concentrations measured at the ARM site, but it is
380 lower than observed OA values by ~24% during Sept-Oct and ~30% annually. For the period of
381 interest, the model simulates a large fire signal in August that is not seen in the measurements.
382 However, this strong August biomass burning signal does show up in the GoAmazon CO
383 measurements (Figure 1b). Generally, it is challenging for a model to capture an aerosol plume,
384 particularly one from biomass burning, at the right time and location due to the aerosols' high
385 spatial inhomogeneity and short lifetime.

386



387

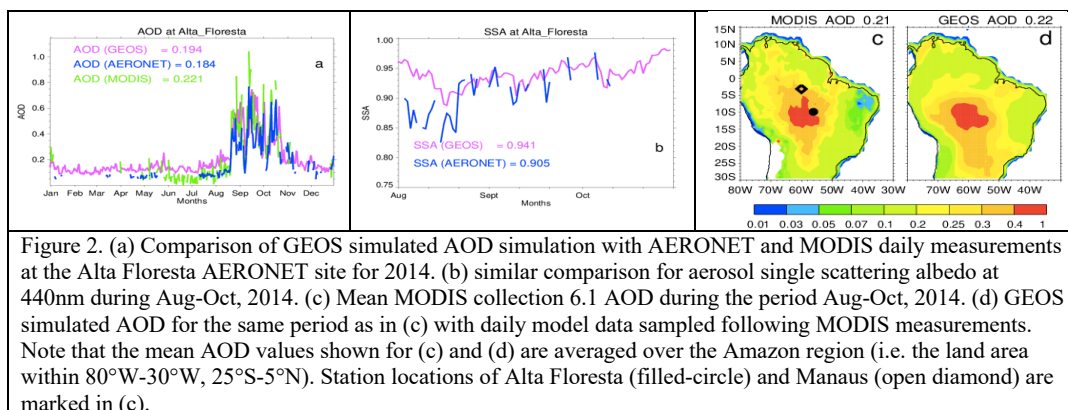


Figure 2. (a) Comparison of GEOS simulated AOD simulation with AERONET and MODIS daily measurements at the Alta Floresta AERONET site for 2014. (b) similar comparison for aerosol single scattering albedo at 440nm during Aug-Oct, 2014. (c) Mean MODIS collection 6.1 AOD during the period Aug-Oct, 2014. (d) GEOS simulated AOD for the same period as in (c) with daily model data sampled following MODIS measurements. Note that the mean AOD values shown for (c) and (d) are averaged over the Amazon region (i.e. the land area within 80°W-30°W, 25°S-5°N). Station locations of Alta Floresta (filled-circle) and Manaus (open diamond) are marked in (c).

388

389 When compared with aircraft G-1 measurements over a $\sim 2^\circ \times 2^\circ$ region around the center of
390 Manaus during the biomass burning season (Sept. 6 – Oct. 4, 2014) (Figure 1c), the simulated
391 vertical OA concentrations underestimate the measurements in the free troposphere but
392 overestimate them in the boundary layer, although they overlap within their standard deviations
393 for all altitudes. Here the model data have been sampled spatially and temporally along the G-1
394 flight paths. This surface OA overestimation by the model seems to contradict the model's
395 underestimation seen in Figure 1a, indicating again that capturing aerosols at the right times and
396 locations is a challenge.

397

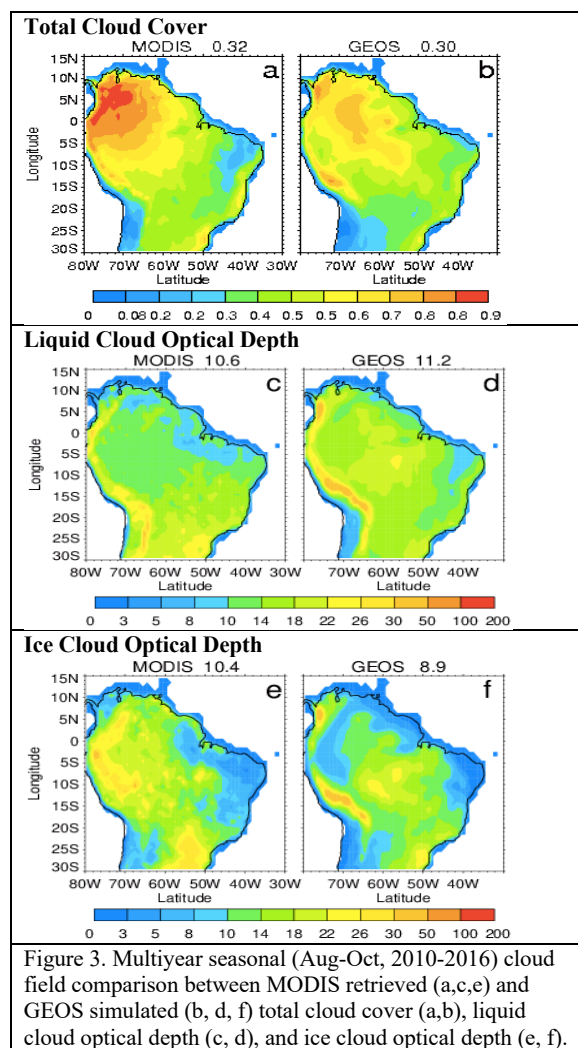
398 Figure 2 shows the AOD (550nm) and SSA (440nm) comparison at a specific station and over
399 South America. We consider AERONET observational data at Alta_Floresta, which is located
400 close to the central Amazon fires (The location is marked in Figure 2c as a filled-in circle). The
401 model-simulated, AERONET-measured, and MODIS-retrieved AOD at this site agree within
402 20% (Figure 2a), and all show a peak of AOD during the biomass burning season. SSA during
403 the burning season generally ranges between 0.85 – 0.95 (Figure 2b). The model agrees with the
404 measurements well except during the first half of August, when the model aerosols are too
405 scattering. However, it is puzzling to observe the extremely low measured SSA in the beginning
406 of August given that the AOD is still low then, as shown in Figure 2a. Regionally over the
407 Amazon region, defined throughout the study as the land area within 80°W-30°W, 25°S-5°N, the
408 model-simulated AOD (0.22 in Figure 2d) during the biomass burning season generally agrees
409 with MODIS satellite retrievals (0.21 in Figure 2c). A simulated high bias is seen over the east
410 Amazon; however, though this region is in our area of interest, the bias should have only a minor
411 impact on our study given that the area is relatively bare, with little vegetation coverage.

412

413 The accurate simulation of cloud fields is also important for our study. In Figure 3 we evaluate
414 the GEOS-simulated cloud cover fraction and cloud optical depth with MODIS satellite
415 products. Here the GEOS data have been sampled with MODIS overpass time and location.
416 GEOS generally captures the magnitude and main features of the cloud fields observed in
417 MODIS, though with some differences; the model overestimates the cloud quantities over the
418 central Amazon and underestimates them in northwest South America. The overall difference
419 over the Amazon region between simulated and MODIS-based estimates is less than 7% for
420 cloud cover fraction, 10% for liquid water cloud optical depth, and 15% for ice cloud optical



421 depth. It is worth mentioning that cloud quantities are notoriously difficult to retrieve over the
422 Amazon, and thus these differences are within the margin of error of the retrievals.
423



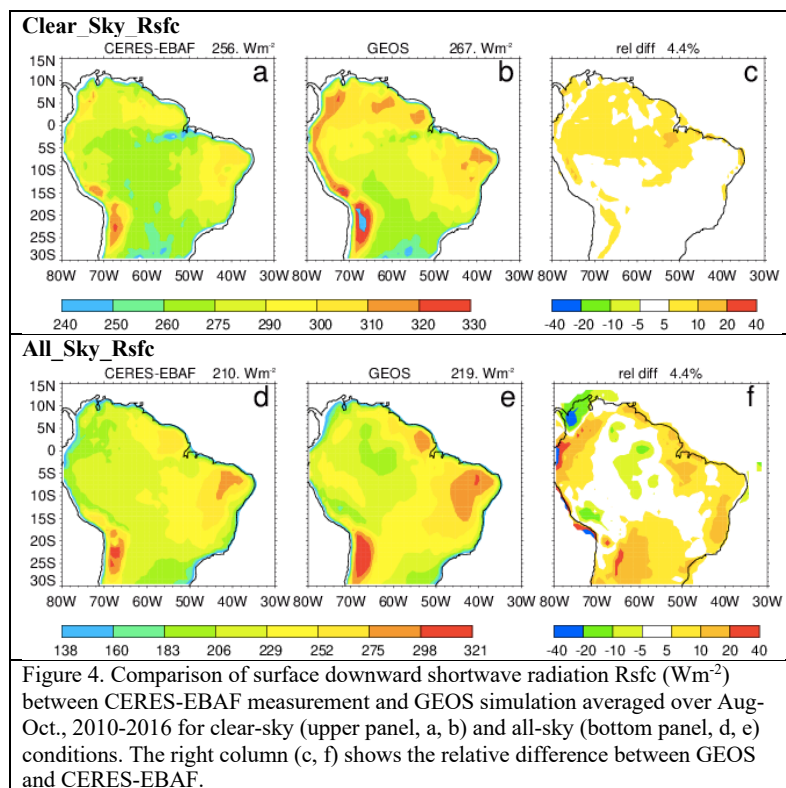
457

458 Figure 4 shows a comparison between the simulated downward shortwave radiation at the
459 surface and CERES-EBAF measurements averaged over Aug-Oct., 2010-2016 for both clear-sky
460 and all-sky conditions. GEOS captures the observed spatial patterns with ~4% high bias for both
461 clear and all sky conditions over the Amazon region.
462

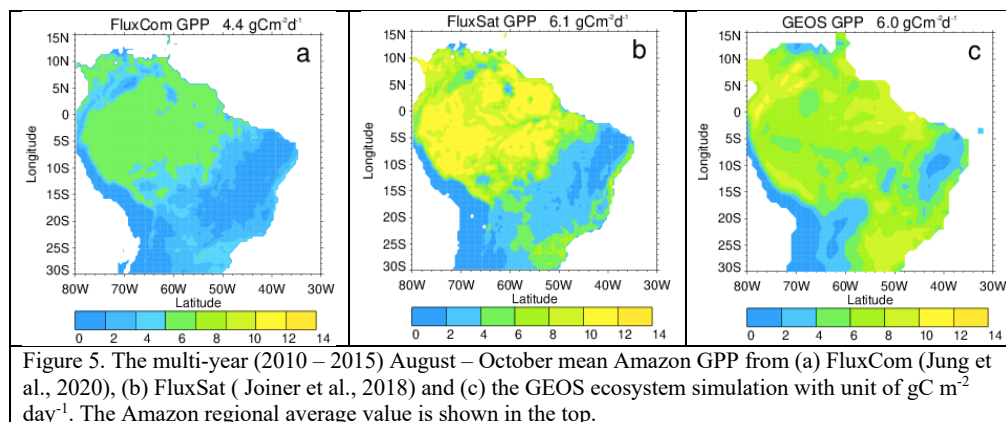
463
464
465
466



467



468



469

470 Figure 5 shows GPP averaged over August to October of 2010-2015 from the two observations-
 471 based products (i.e., FluxCom and FluxSat) and the GEOS simulation. As we mentioned in
 472 section 2.2, FluxCom GPP is derived from surface measurements of carbon fluxes while FluxSat
 473 GPP is derived from satellite data. The overall spatial distributions of GEOS GPP (Figure 5c)
 474 over South America are similar to both of the observations-based datasets (Figures 5a and 5b)



475 with higher values over the eastern part of the domain but lying between the two datasets in other
476 areas. Over the studied period and the Amazon region, the GEOS GPP is comparable to the
477 FluxSat GPP and is about 35% higher than the FluxCom GPP.

478

479

3.2 Principle of aerosol and cloud impact on surface downward radiation

480

481

482

483

484

485

486

487

488

489

490

491

492

493

494

495

496

497

498

Radiative responses to aerosols and cloud fields are nonlinear. To better explain the phenomenon examined here – that plant growth increases at low-to-intermediate AOD but decreases at high AOD – we ran the column version of a radiation model, fast-JX (Bian and Prather, 2002). The model calculations provide two ratios: (i) CI_{dir} , the ratio of direct downward solar radiation at the surface (R_{dir}) to the incoming total solar radiation flux at the top of the atmosphere (R_{top}), and (ii) CI_{diff} , the ratio of the downward diffuse solar radiation flux (R_{diff}) to R_{top} . Results for different biomass burning AODs (including the clean air condition, where $AOD = 0$) for cloud-free conditions are shown in Figure 6a. When the sky is clear and clean (both cloud-free and without aerosols), roughly 90% of the incoming solar radiation at the top of the atmosphere can reach the plant canopy (i.e., $CI_{dir} + CI_{diff} \approx 0.9$ at $BBAOD = 0$). The direct solar flux decreases rapidly as the atmosphere becomes polluted (i.e., as $BBAOD$ increases), but for $BBAOD$ levels less than ~ 0.75 , the majority of this reduction is compensated by an increase in the diffuse solar flux. The two are equivalent at $AOD \sim 0.5$. This light redistribution from direct to diffuse can significantly stimulate plant photosynthesis given that plants use diffuse light more efficiently. Ecosystems could still respond positively to increasing $BBAOD$ even if the incident diffuse radiation diminishes below its peak value, though for some value of $BBAOD$, the reduction in total radiation will be large enough to overwhelm the impact of increased diffuse radiation, and plant photosynthesis will be lower than that for clean sky conditions.

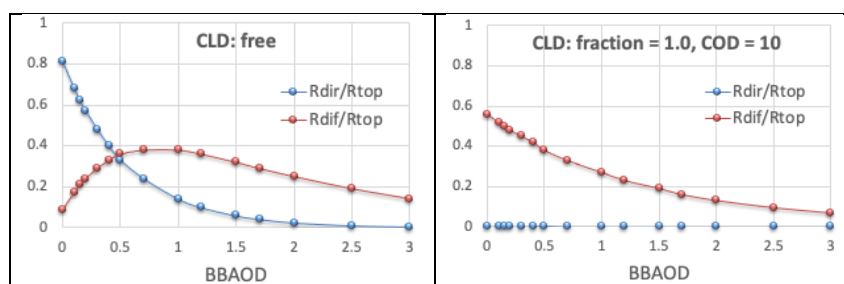


Figure 6. The ratio of R_{dir} to R_{top} (blue), which presents clearness index of direct radiation portion (CI_{dir}) and the ratio of R_{diff} to R_{top} (red) for diffuse radiation portion (CI_{diff}). Here, R_{top} is incoming total solar flux at the top of atmosphere (TOA), R_{dir} is surface downward direct solar flux, and R_{diff} is surface downward diffuse solar flux. All R_s are over 400-700 nm. Left: there is a layer of biomass burning derived aerosol varying in AOD (BBAOD) under clear sky condition. Note that when $BBAOD = 0$, the sky is clear and clean. Right: atmosphere has a layer of biomass burning aerosol underneath a layer cloud with the cloud fraction 1.0 and cloud optical depth of 10. Calculations use fast-JX radiation model column version adopting a standard atmospheric condition of typical tropics at ozone column = 260 DU, $SZA = 15^\circ N$ and surface albedo = 0.1.

499

500

501

502

The Amazon dry season is characterized by high biomass burning aerosol loading combined with low cloud cover, a good match to obtain more diffuse radiation without the loss of too much total radiation. However, as we have pointed out, cloud impacts on radiation typically dominate those

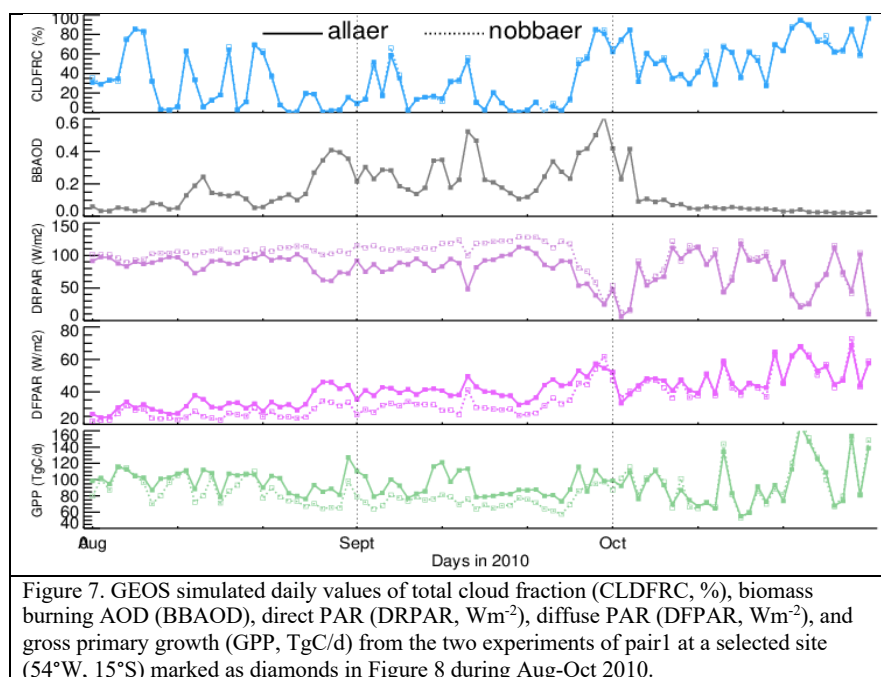


503 of aerosols. To examine this, we repeated the radiation model calculations after adding, at the top
504 of the aerosol layer, a cloud layer with a cloud fraction of 1.0 and a cloud optical depth (COD) of
505 10, which is close to the mean liquid cloud COD over the Amazon dry season (Figure 3). The
506 impact on R_{dir} and R_{diff} is quite large (Figure 6b). Without BBAer, the clouds already fill the sky
507 with abundant diffuse light that can reach the surface (i.e., $CI_{\text{diff}} > 50\%$), while almost shutting
508 down the direct light (i.e., $CI_{\text{dir}} < 1\%$). Accordingly, for full cloud coverage, a clean sky (i.e., no
509 aerosols) would provide the best conditions for plant growth. When fires start, the diffuse light
510 declines rapidly, reducing the potential for plant growth. At BBAOD ~ 3 the two curves look
511 similar, that is essentially no radiation at the surface.

512 The simple examples in Figure 6 illustrate the complicated responses of direct and diffuse light
513 to the presence of aerosol and cloud. Measurements indicate that plant growth peaks for a
514 clearness index (CI, defined as $CI_{\text{dir}} + CI_{\text{diff}}$) of about 0.4-0.7 for some forest ecosystems (Butt
515 et al., 2010, Letts and Lafleur, 2005). This CI range translates, based on Figure 6, to a BBAOD
516 range of about 0.3~1.5 in clear sky and 0~0.5 in cloudy-sky conditions.

518 3.3 How the ecosystem responds to the BBAer light fertilizer effect

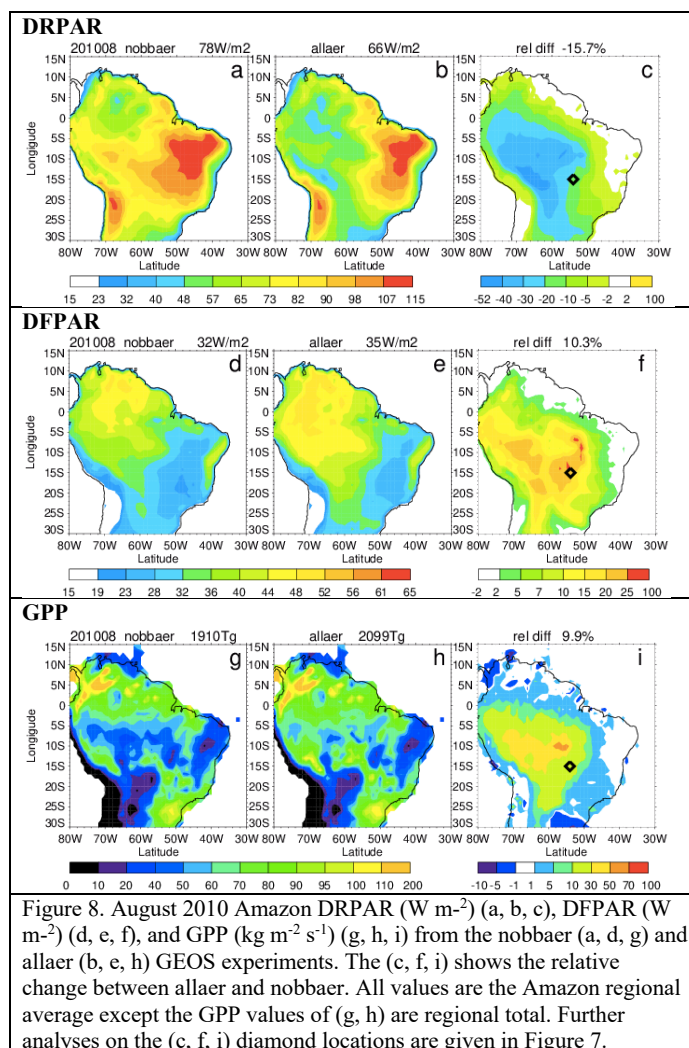
519 We first examine the two pair1 experiments by taking a close look at the time series of aerosol,
520 cloud, radiation, and ecosystem responses generated at a selected site (54°W , 15°S) during Aug-
521 Oct 2010 (Figure 7) (site location marked in Figure 8), with the aim of extending the general
522



523 understanding gained in section 3.2 to a real case study at a single site in the Amazon. This is an
524 interesting site and period, showing a large DFPAR change (Figure 8f) and providing a wide
525 variety of conditions for study – the sky alternates between clear and cloudy conditions in
526 August, is relatively clear in September, and is relatively cloudy in October, and the biomass
527



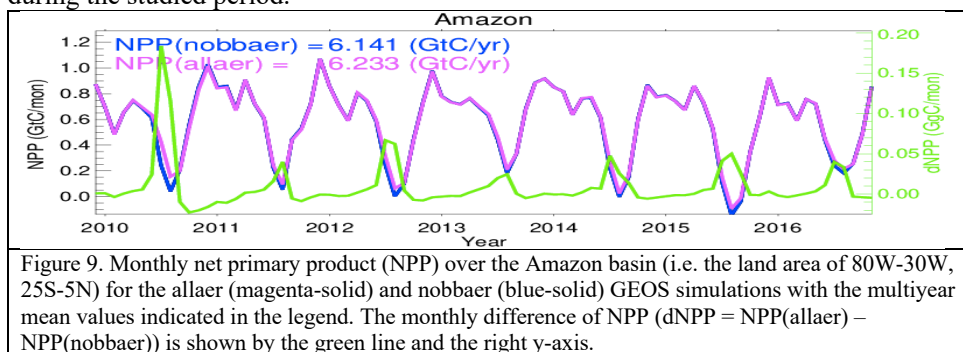
528 burning aerosols increase in August, peak in September, and diminish greatly in early October
 529 (Figure 7). During August-September, when the atmosphere experiences biomass burning
 530 pollution, the allaer (with BBAOD light fertilizer) and nobbaer (without BBAOD light fertilizer)
 531 results differ significantly: DRPAR for allaer (solid line) lies below that for nobbaer (dotted-
 532 line), while DFPAR and GPP for allaer are generally higher than those for nobbaer. In October,
 533 the sky is almost clean (i.e., low BBAer), leading to very similar results for DRPAR, DFPAR,
 534 and GPP between the two experiments. Looking closer, we see that the changes of DRPAR,
 535 DFPAR, and GPP between allaer and nobbaer are more prominent when the atmosphere has low
 536 cloudiness and high aerosol (e.g., at the end of August), confirming both that BBAer does
 537 transform some of the direct light at the surface into diffuse light and that plants are more
 538 efficient in their use of diffuse light. When both cloudiness and aerosols are high (e.g., at the end
 539 of September), the influence of aerosols is overwhelmed by clouds, and the impact of the
 540 aerosols on radiation and the ecosystem becomes secondary.





574 We now evaluate BB aerosol impacts on radiation and ecosystem fields over the Amazon during
575 August 2010, when the aerosol has its largest impact. Figure 8 shows the simulated Amazon
576 DRPAR, DFPAR, and GPP fields from the two experiments comprising pair1 (nobbaer and
577 allaer). The distribution of DRPAR shows a clear spatial gradient, with low values in the
578 northwest and high values in the southeast, and the spatial pattern of DFPAR shows the reverse
579 pattern. These features are primarily controlled by the cloud distribution (Figure 3). Comparing
580 the nobbaer and allaer results by calculating field relative change (i.e., (allaer-nobbaer)/allaer),
581 we find that BBAer decreases DRPAR by 16% and increases DFPAR by 10% over the Amazon
582 region, with maximum local changes of up to -50% for DRPAR and 25% for DFPAR.
583 Interestingly, these maxima are not co-located, though the spatial patterns of perturbations do
584 agree with each other. The mismatch in the locations of the maxima in the difference fields
585 implies a nonlinear response of direct and diffuse light to aerosol and cloud particles (see section
586 3.2). In response to the inclusion of BBAer, the Amazon GPP increases by 10%. That is, the
587 increase in GPP stemming from the increase in the diffuse light fraction overwhelms a potential
588 reduction in GPP from a reduction of total PAR.
589

590 We also examine the multi-year (2010-2016) BBAer impacts on net primary production (NPP),
591 that is, the rate at which carbon is accumulated (GPP) in excess of autotrophic respiration. In
592 essence, NPP can be considered a proxy for the net plant sink of atmospheric carbon. Figure 9
593 shows monthly and long-term averaged NPP over the Amazon Basin from the two experiments
594 comprising pair1. The monthly change of NPP (i.e., $dNPP = NPP(\text{allaer}) - NPP(\text{nobbaer})$) is
595 shown in the figure as a green line. Each year, during the August-September period when BBAer
596 is high and cloudiness is low over the Amazon, BBAer is seen to enhance NPP. The percentage
597 difference of annually-averaged NPP ($dNPP/NPP(\text{nobbaer}) * 100$) in % is 4.2, 0.06, 1.9, 0.5, 1.3,
598 1.9, and 1.0 for the seven studied years. That means the BBAer-induced NPP increases range
599 from 5 TgC yr⁻¹ or 0.06% (2011) to 278 TgC yr⁻¹ or 4.2% (2010), with a seven-year average of
600 92 TgC or 1.5%. This is equivalent to storing 92TgC annually within the Amazon ecosystem
601 during the studied period.



602
603 The CO₂ fire emission data from the GFED4.1s emission inventory indicate that over this area
604 and time period, fires emit ~250TgCyr⁻¹. The NPP enhancement due to the BBAer-induced
605 diffuse sunlight fertilization thus compensates for about 37% of carbon loss by fires. Our
606 estimates of NPP increases across the Amazon region have a larger interannual range (0.5-4.2%)
607 than that (1.4-2.8%) reported by Rap et al. (2015), although our seven-year averaged NPP
608 increase (1.5%) lies within their range. This is consistent with our study's use of a larger
609 interannual variation of biomass burning emissions into the real atmosphere (e.g., ~ 6x



610 interannual difference in Amazon OC emission during Aug-Sept, 2010-2016, compared to 3x
611 assumed in Rap et al. (2015)).

612

613

3.4 How clouds adjust the BBAer sunlight fertilizer effect

614

615

616

617

618

619

620

621

622

623

624

625

626

627

628

629

630

631

Our second objective in this study is to investigate how the presence of clouds affects the ability of BBAer to affect GPP. We highlight the cloud impact because even at the same biomass burning aerosol optical depth (BBAOD), the surface downward DRPAR and DFPA can be very different between cloudy and cloud-free conditions (see section 3.2). As mentioned above, the Amazon's so-called "dry season" still features a considerable amount of cloud, and the cloudiness levels vary significantly from year to year. This raises some questions: How do clouds affect the aerosol impact on radiation fields during the Amazon biomass burning season? Could different levels of background clouds have different impacts on the efficacy of the BBAer light fertilizer effect? Here, to quantify the cloud influence, we examine BBAer impacts during clear-sky (cloud cover < 0.1), cloudy-sky (cloud cover 0.1-0.3, 0.3-0.6 and >0.6), and all-sky conditions based on gridded daily cloud cover over the Amazon region. Figure 10 provides monthly averaged fields of cloud, aerosol, radiation, and GPP over the Amazon basin during the seven years from the two pair1 experiments, with results for the five cloudiness conditions shown separately. The numbers marked in (a)-(d) are the percentage occurrence frequency of the corresponding cloud cover over the Amazon basin in each month. The differences in the radiation and ecosystem quantities between the two pair1 experiments (shown as dotted lines) are labeled as dDRPAR, dDFPAR, and dGPP.

632

633

634

635

636

637

638

639

640

641

642

643

644

Generally, the curves for BBAOD (solid black line) and dGPP (dotted light-blue line) are strongly (and positively) correlated, from $R = 77.4\%$ for cloud cover > 0.6 (Figure 10d) to $R > 94.5\%$ for the four other cloudiness conditions (Figure 10a-c, e). This indicates that interannual changes in dGPP are primarily controlled by interannual fluctuations of biomass burning aerosols. The correlation presumably stems from the fact that biomass burning aerosols increase the diffuse PAR reaching the canopy (dotted pink line) although they decrease the total PAR (dotted purple line) via decreasing direct PAR (Table S1a). This aerosol-radiation-GPP relationship is seen to vary with cloud amount, with clouds acting to reduce the aerosol impact; both the diffuse radiation and the GPP show larger changes with BBAOD under clear sky conditions. The overall (i.e., all-sky) aerosol impact on dGPP is similar to that for a cloud coverage of 0.3-0.6, presumably because the averaged cloud coverage over the Amazon during the studied period is roughly in that range.

645

646

647

648

649

650

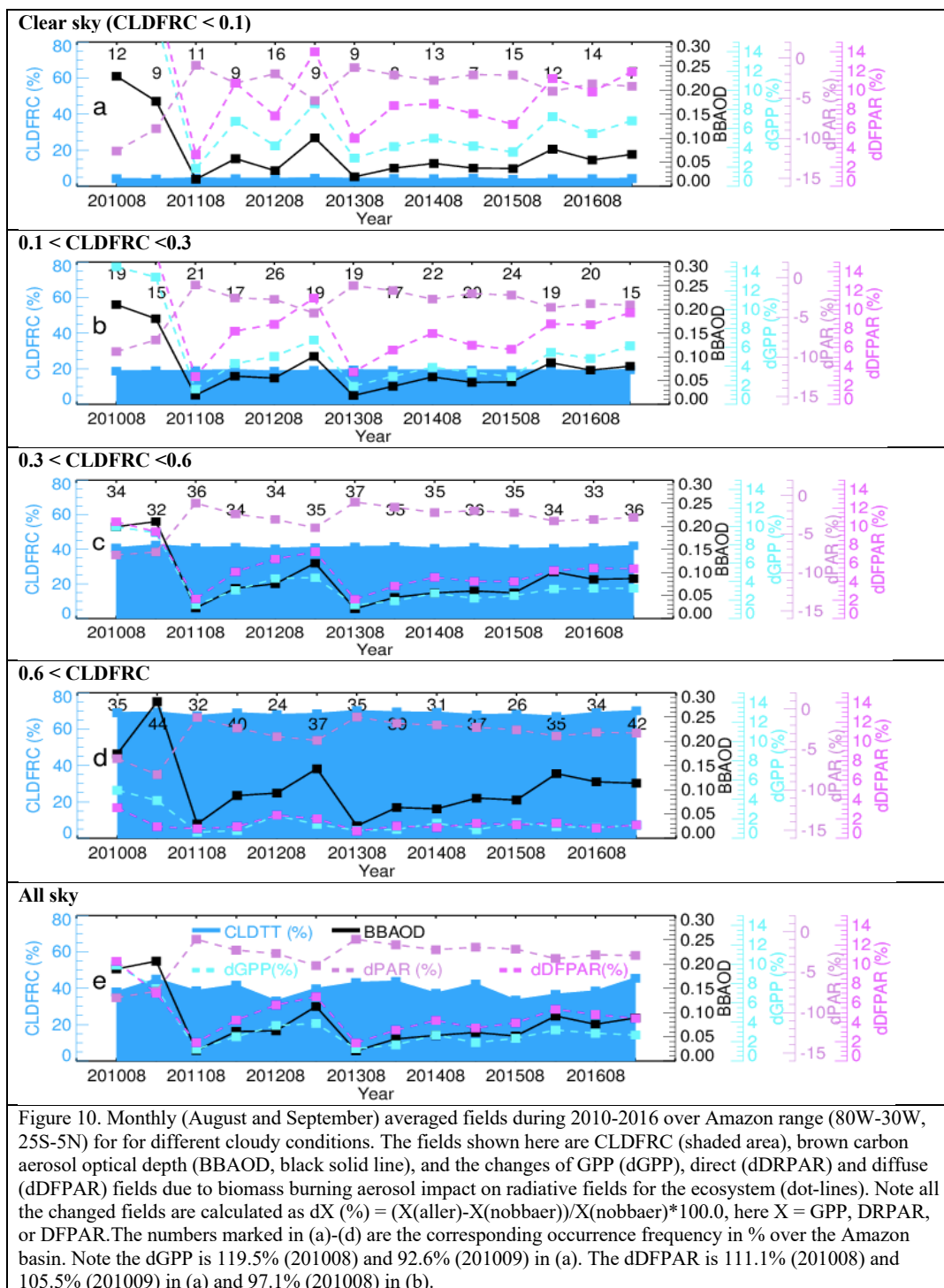
651

652

653

654

Figure 10 and Table S1e show that on an interannual (dry season) basis, the aerosol light fertilizer effect differed the most between 2010 and 2011 (i.e., the dGPP was 8.7% in 2010 and 1.8% in 2011). During these two years, the cloud fraction (CLDFRC) decreased slightly from 42% (2010) to 41% (2011), but BBAOD decreased significantly, by about 80% from 0.198 in 2010 to 0.042 in 2011. Thus, although cloudiness does temper the impact of aerosols on radiation and the ecosystem, the interannual variations of cloudiness in the Amazon (at least during the period we studied) have only a secondary impact on the interannual variations of the aerosol light fertilizer effect. The interannual variation of the aerosol light fertilizer effect is primarily controlled by variations in biomass burning aerosols (e.g., > 6 times variation of biomass burning emissions and BBAOD, table S1e).

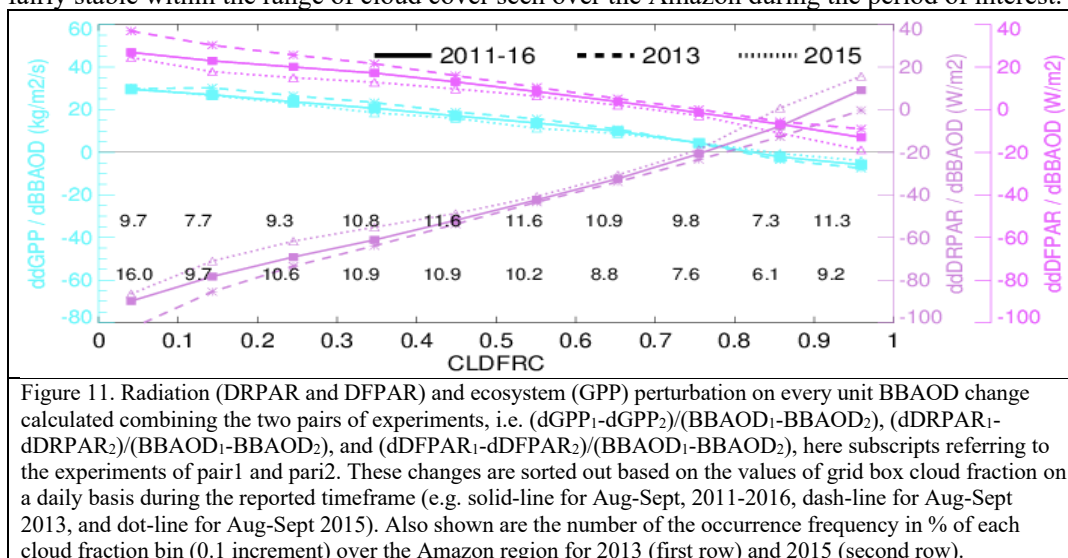




656
 657 Recall, the pair2 experiments are equivalent to the pair1 experiments except for the prescription
 658 of 2010 BB emissions for each year during 2011-2016. By jointly analyzing pair1 and pair 2, we
 659 can quantify the impacts of two different sets of BB emissions under the same meteorological
 660 conditions for every day of every year starting in 2011. Here we study the sensitivity of the
 661 aerosol light fertilizer effect to a unit change of BBAOD. That is, on a daily basis, the sensitivity
 662 of a variable X to a change in the biomass burning AOD is calculated as: $ddX/dBBAOD =$
 663 $((dX)_1 - (dX)_2) / (BBAOD_1 - BBAOD_2)$. Here, the X represents GPP, DRPAR, and DFPAR, and the
 664 subscripts 1 and 2 represent the pair1 or pair2 experiment, respectively.
 665

666 $ddX/dBBAOD$ is computed on a gridded daily basis over August-September of 2011-2016.
 667 The calculations are then catalogued according to daily cloud cover fraction – we combine
 668 the results within each of 10 cloud fraction bins (0-0.1, 0.1-0.2, ..., 0.9-1.0). To examine the
 669 maximum impact of interannual cloud change during our study period, the binned
 670 $ddX/dBBAOD$ vs. CLDFRC relationship is also computed separately from daily (August-
 671 September) values in 2013 and from corresponding daily values in 2015, as these are the
 672 years for which monthly cloud cover is around the maximum (0.44) and minimum (0.35),
 673 respectively (Figure 10 and table S1e).

674
 675 Figure 11 shows the results. An almost linear relationship is seen between the $ddX/dBBAOD$
 676 values and cloud cover fraction. BB aerosols increase GPP in clear sky conditions (e.g., 29.6
 677 $kgm^{-2}s^{-1}$) but decrease it under full cloudiness conditions (e.g., $-5.8 kgm^{-2}s^{-1}$). The cloud fraction
 678 at which BB aerosol switches from stimulating to inhibiting plant growth occurs at ~ 0.8 . Cloud
 679 conditions thus not only affect strongly the strength of the aerosol light fertilizer effect but can
 680 also change the fundamental direction of the effect. The lines produced for the three different
 681 study periods are fairly similar, indicating that the relationship of $ddX/dBBAOD$ to CLDFRC is
 682 fairly stable within the range of cloud cover seen over the Amazon during the period of interest.



683



684 4. Conclusions

685 We use the NASA GEOS ESM system with coupled aerosol, cloud, radiation, and ecosystem
686 modules to investigate the impact of biomass burning aerosols on plant productivity across the
687 Amazon Basin under the natural background cloud fields experienced during 2010-2016 – a
688 period containing a broad range of cloudiness conditions. We find that the biomass burning
689 aerosol light fertilizer effect does stimulate plant growth and has a notable impact on Amazon
690 ecosystem productivity during the biomass burning season (August-September). In the long-term
691 mean, the aerosol light fertilizer increases DFPAR by 3.8% and decreases DRPAR by 5.4%,
692 allowing it to increase Amazon GPP by 2.6%. On a monthly basis, the light fertilizer effect can
693 increase GPP by up to 9.9%. Consequently, biomass burning aerosols increase Amazonia yearly
694 NPP by 1.5% on average, with yearly increases ranging from 0.06% to 4.2% over the seven
695 years studied. This 1.5% NPP enhancement (or $\sim 92\text{TgC yr}^{-1}$) is equivalent to $\sim 37\%$ of the carbon
696 loss due to Amazon fires.

697
698 The aerosol light fertilizer effect is strongly dependent on the presence of clouds, much stronger
699 in clear sky conditions and decreases with the increase of cloudiness. A fairly robust linear
700 relationship is found between cloud cover fraction and the sensitivity of radiation and GPP
701 change to a change in biomass burning AOD. Curiously, BB aerosols stimulate plant growth
702 under clear-sky conditions but suppress it under full cloudiness conditions. The cloud fraction at
703 which BB aerosol switches from stimulating to inhibiting plant growth occurs at ~ 0.8 . Note,
704 however, that while our results show a clear sensitivity of the aerosol light fertilizer effect to
705 cloudiness, interannual variations in the aerosol light fertilizer's overall effectiveness are
706 controlled primarily by interannual variations in biomass burning aerosols during our studied
707 period because biomass burning AOD can vary by a factor of 6 from year to year. The associated
708 large variations in BBAOD are inevitably propagated to the radiation and ecosystem fields.
709 Overall, our work indicates that feedbacks between aerosols, radiation, and the ecosystem need
710 to be performed in the context of an atmospheric environment with a cloud presence.

711
712 This study examines the potential for the biomass burning aerosol light fertilizer effect to
713 stimulate growth in unburned forest over the Amazon basin. The net feedback of Amazon fires
714 on the Amazon biome is still an open question. Some changes, such as increasing atmospheric
715 CO_2 and aerosols, serve as forest fertilizers, whereas others, such as increasing O_3 pollution
716 levels and the deposition of smoke particles on plant leaves, reduce plant photosynthesis. On top
717 of this, fires also induce changes in meteorological fields (e.g., temperature, precipitation,
718 clouds) that can affect plant growth. More efforts are needed to investigate the ecosystem effect
719 of Amazon fires by integrating all these potential factors.

720 721 **Acknowledgements:**

722 The authors thank the various observational groups (i.e., AERONET, CERES-EBAF, FluxCom,
723 FluxSat, and GoAmazon). HB was supported by the NASA ACMAP funding (no.
724 NNX17AG31G). PRC was supported by the Chemistry-Climate Modeling workpackage funded
725 by the NASA Modeling, Analysis, and Prediction program (David Considine, program
726 manager). JES was supported by the by the U.S. Department of Energy's Atmospheric System
727 Research, an Office of Science Biological and Environmental Research program; PNNL is
728 operated for the DOE by Battelle Memorial Institute under contract DE-AC05-76RL01830.



729 Resources supporting this work were provided by the NASA GMAO SI-Team and the High-End
730 Computing (HEC) Program through the NASA Center for Climate Simulation (NCCS) at
731 Goddard Space Flight Center (GSFC). FluxSat data were provided by Joanna Joiner group in
732 GSFC. GoAmazon data were obtained from the Atmospheric Radiation Measurement (ARM)
733 user facility, a US Department of Energy (DOE) Office of Science User facility managed by the
734 Biological and Environmental Research program.

735

736 **Data Availability:**

737 All of the observational data used in this study are publicly accessible, e.g., AERONET
738 (<https://aeronet.gsfc.nasa.gov>), CERES-EBAF (<https://ceres.larc.nasa.gov/data/>), FluxCom
739 (<http://www.fluxcom.org>), FluxSat (<https://avdc.gsfc.nasa.gov>), and GoAmazon
740 (<https://www.arm.gov/research/campaigns/amf2014goamazon>). The GEOS model results can be
741 provided by contacting with the corresponding author.

742

743 **Author contributions:**

744 H.B. took an overall responsible for the experiment design, model simulation, and data analysis.
745 E.L., R. D. K., S. P. M., and F. Z. contributed to the ecosystem study, D. O. B. contributed to the
746 cloud study, M. C., P. R. C., A. S. D, M. E. M., and H. Y. contributed to the aerosol study and
747 the model-observation comparison, P. N. contribute to the radiation study, and J. S. provided the
748 GoAmazon results. All authors contributed to the paper writing.

749

750 **References:**

- 751 Abdul-Razzak, H. and Ghan, S.: A parameterisation of aerosol activation 2. Multiple aerosol types, *J.*
752 *Geophys. Res.*, 105, 6837–6844, 2000.
- 753 Barahona, D. and Nenes, A.: Parameterizing the competition between homogeneous and heterogeneous
754 freezing in cirrus cloud formation – monodisperse ice nuclei, *Atmos. Chem. Phys.*, 9, 369–381,
755 doi:10.5194/acp-9-369-2009, 2009
- 756 Barahona, D., Molod, A., Bacmeister, J., Nenes, A., Gettelman, A., Morrison, H., Phillips, V., and
757 Eichmann, A.: Development of two-moment cloud microphysics for liquid and ice within the NASA
758 Goddard Earth Observing System Model (GEOS-5), *Geoscientific Model Development*, 7, 1733–
759 1766, 2014.
- 760 Bian, H., and M. J. Prather, Accurate simulation of stratospheric photolysis in global chemical model. *J.*
761 *Atmos. Chem.*, 41, 281-296, 2002.
- 762 Bian, H., M. Chin, S. R. Kawa, H. Yu, T. Diehl (2010), Multi-scale carbon monoxide and aerosol
763 correlations from MOPITT and MODIS satellite measurements and GOCART model: implication for
764 their emissions and atmospheric evolutions, *J. Geophys. Res.*, 115, D07302,
765 doi:10.1029/2009JD012781.
- 766 Bian, H., P. Colarco, M. Chin, G. Chen, J. M. Rodriguez, Q. Liang, D. Blake, D. A. Chu, A. da Silva, A.
767 S. Darmenov, G. Diskin, H. E. Fuelberg, G. Huey, Y. Kondo, J. E. Nielsen, X. Pan, and A. Wisthaler
768 (2013), Source attributions of pollution to the western Arctic during the NASA ARCTAS field
769 campaign, *Atmos. Chem. Phys.*, 13, 4707–4721.
- 770 Bian, H., M. Chin, D. A. Hauglustaine, M. Schulz, G. Myhre, S. E. Bauer, M. T. Lund, V. A. Karydis, T.
771 L. Kucsera, X. Pan, A. Pozzer, R. B. Skeie, S. D. Steenrod, K. Sudo, K. Tsigaridis, A. P. Tsimpidi,
772 and S. G. Tsyro (2017), Investigation of global particulate nitrate from the AeroCom phase III
773 experiment *Atmos. Chem. Phys.*, 17, 12911–12940 ([https://www.atmos-chem-](https://www.atmos-chem-phys.net/17/12911/2017/)
774 [phys.net/17/12911/2017/](https://www.atmos-chem-phys.net/17/12911/2017/)).
- 775 Bian, H., Froyd, K., Murphy, D. M., Dibb, J., Darmenov, A., Chin, M., Colarco, P. R., da Silva, A.,
776 Kucsera, T. L., Schill, G., Yu, H., Bui, P., Dollner, M., Weinzierl, B., and Smirnov, A.:



- 777 Observationally constrained analysis of sea salt aerosol in the marine atmosphere, *Atmos. Chem.*
778 *Phys.*, 19, 10773–10785, <https://doi.org/10.5194/acp-19-10773-2019>, 2019.
- 779 Breen, K. H., D. Barahona, T. Yuan, H. Bian, and S. C. James, Effect of volcanic emissions on
780 clouds during the 2008 and 2018 Kilauea degassing events, [https://doi.org/10.5194/acp-2020-](https://doi.org/10.5194/acp-2020-979)
781 [979](https://doi.org/10.5194/acp-2020-979), 2020.
- 782 Butt, N., M. New, Y. Malhi, A. C. Lola da Costa, P. Oliveira, and J. E. Silva-Espejo (2010), Diffuse
783 radiation and cloud fraction relationships in two contrasting Amazonian rainforest sites, *Agric. For.*
784 *Meteorol.*, 150(3), 361–368.
- 785 Carn, S., Fioletov, V., McLinden, C. *et al.* A decade of global volcanic SO₂ emissions measured from
786 space. *Sci Rep* 7, 44095 (2017). <https://doi.org/10.1038/srep44095>.
- 787 Chin, M., T. Diehl, O. Dubovik, T. F. Eck, B. N. Holben, A. Sinyuk, and D. G. Streets (2009), Light
788 absorption by pollution, dust and biomass burning aerosols: A global model study and evaluation
789 with AERONET data, *Ann. Geophys.*, 27, 3439-3464.
- 790 Chin, M., Diehl, T., Tan, Q., Prospero, J. M., Kahn, R. A., Remer, L. A., Yu, H., Sayer, A. M., Bian, H.,
791 Geogdzhayev, I. V., Holben, B. N., Howell, S. G., Huebert, B. J., Hsu, N. C., Kim, D., Kucsera, T. L.,
792 Levy, R. C., Mishchenko, M. I., Pan, X., Quinn, P. K., Schuster, G. L., Streets, D. G., Strode, S. A.,
793 Torres, O., and Zhao, X.-P.: Multi-decadal aerosol variations from 1980 to 2009: a perspective from
794 observations and a global model, *Atmos. Chem. Phys.*, 14, 3657–3690, [https://doi.org/10.5194/acp-](https://doi.org/10.5194/acp-14-3657-2014)
795 [14-3657-2014](https://doi.org/10.5194/acp-14-3657-2014), 2014.
- 796 Colarco, P. R., A. da Silva, M. Chin, T. Diehl (2010), Online simulations of global aerosol distributions in
797 the NASA GEOS-4 model and comparisons to satellite and ground-based aerosol optical depth, *J.*
798 *Geophys. Res.*, 115, D14207, doi:10.1029/2009JD012820.
- 799 Colarco, P. R., Gassó, S., Ahn, C., Buchard, V., Dasilva, A. M., & Torres, O. (2017). Simulation of the
800 Ozone Monitoring Instrument aerosol index using the NASA Goddard Earth Observing System
801 aerosol reanalysis products. *Atmospheric Measurement Techniques*. [https://doi.org/10.5194/amt-10-](https://doi.org/10.5194/amt-10-4121-2017)
802 [4121-2017](https://doi.org/10.5194/amt-10-4121-2017).
- 803 Cirino, G. G., R. A. F. Souza, D. K. Adams, and P. Artaxo, The effect of atmospheric aerosol particles
804 and clouds on net ecosystem exchange in the Amazon, *Atmos. Chem. Phys.*, 14, 6523–6543, 2014,
805 www.atmos-chemphys.org.
- 809 Doughty, C. E., M. G. Flanner, and M. L. Goulden (2010), Effect of smoke on subcanopy shaded light,
810 canopy temperature, and carbon dioxide uptake in an Amazon rainforest, *Global Biogeochem.*
811 *Cycles*, 24, GB3015, doi:10.1029/2009GB003670.
- 812 Doughty, C.E., Metcalfe, D.B., Girardin, C.A.J., Farfan-Amezquita, F., Galiano Cabrera, D., Huaraca
813 Huasco, W. et al. (2015). Drought impact on forest carbon dynamics and fluxes in Amazonia. *Nature*,
814 519:78–82.
- 815 Doughty, Russell, Philipp Köhler, Christian Frankenberg, Troy S. Magney, Xiangming Xiao, Yuanwei
816 Qin, Xiaocui Wu, Berrien Moore. TROPOMI reveals dry-season increase of solar-induced
817 chlorophyll fluorescence in the Amazon forest. *Proceedings of the National Academy of Sciences*,
818 2019; 201908157 DOI: [10.1073/pnas.1908157116](https://doi.org/10.1073/pnas.1908157116).
- 819 Ezhova, E., Ylivinkka, I., Kuusk, J., Komsaare, K., Vana, M., Krasnova, A., Noe, S., Arshinov,
820 M., Belan, B., Park, S. B., Lavrič, J. V., Heimann, M., Petäjä, T., Vesala, T., Mammarella, I., Kolari,
821 P., Bäck, J., Rannik, Ü., Kerminen, V. M., & Kulmala, M. (2018). Direct effect of aerosols on solar
822 radiation and gross primary production in boreal and hemiboreal forests. *Atmospheric Chemistry and*
823 *Physics*, 18(24), 17,863–17,881. <https://doi.org/10.5194/acp-18-17863-2018>.
- 824 Feldpausch, T. R., et al. (2016), Amazon forest response to repeated droughts, *Global Biogeochem.*
825 *Cycles*, 30, 964–982, doi:10.1002/2015GB005133.
- 826 Feng, Y., Chen, D. & Zhao, X. Estimated long-term variability of direct and diffuse solar
827 radiation in North China during 1959–2016. *Theor Appl Climatol* 137, 153–163 (2019).
828 <https://doi.org/10.1007/s00704-018-2579-1>



- 829 Fountoukis, C. and Nenes, A.: Continued development of a cloud droplet formation parameterization for
830 global climate models, *J. Geophys. Res.*, 110, D11212, doi:10.1029/2004JD005591, 2005.
- 831 Gelaro, R., McCarty, W., Suárez, M. J., Todling, R., Molod, A., Takacs, L., et al. (2017). The Modern-
832 Era Retrospective Analysis for Research and Applications, Version 2 (MERRA-2). *Journal of*
833 *Climate*, 30(14), 5419–5454. <https://doi.org/10.1175/JCLI-D-16-0758.1>
- 834 Gu, L. H., D. D. Baldocchi, S. C. Wofsy, J. W. Munger, J. J. Michalsky, S. P. Urbanski, and T. A. Boden
835 (2003), Response of a deciduous forest to the Mount Pinatubo eruption: Enhanced photosynthesis,
836 *Science*, 299(5615), 2035–2038.
- 837 Guenther, A. B., X. Jiang, C. L. Heald, T. Sakulyanontvittaya, T. Duhl, L. K. Emmons and X. Wang
838 (2012). "The Model of Emissions of Gases and Aerosols from Nature version 2.1 (MEGAN2.1): an
839 extended and updated framework for modeling biogenic emissions." *Geosci. Model Dev.* 5(6): 1471-
840 1492.
- 841 Hemes, K. S., Verfaillie, J., and Baldocchi, D. D.: Wildfire-Smoke Aerosols Lead to Increased Light Use
842 Efficiency Among Agricultural and Restored Wetland Land Uses in California's Central Valley, *J.*
843 *Geophys. Res.-Biogeo.*, 125, e2019JG005380, <https://doi.org/10.1029/2019jg005380>, 2020.
- 844 Hodzic A. and Jimenez J.L. (2011), Modeling anthropogenically controlled secondary organic aerosols in
845 a megacity: a simplified framework for global and climate models. *Geosci. Model. Dev.*, 4, 901-917,
846 doi:10.5194/gmd-4-901-2011.
- 847 Huete, A. R., K. Didan, Y. E. Shimabukuro, P. Ratana, S. R. Saleska, L. R. Hutryra, W. Yang, R. R.
848 Nemani, and R.
- 849 Myneni (2006), Amazon rainforests green-up with sunlight in dry season, *Geophys. Res. Lett.*, 33,
850 L06405, doi:10.1029/2005GL025583.
- 851 Iacono, M.J., J.S. Delamere, E.J. Mlawer, M.W. Shephard, S.A. Clough, and W.D. Collins, Radiative
852 forcing by long-lived greenhouse gases: Calculations with the AER radiative transfer models, *J.*
853 *Geophys. Res.*, 113, D13103, doi:10.1029/2008JD009944, 2008.
- 854 Joiner, J., Yoshida, Y., Zhang, Y., Duveiller, G., Jung, M., Lya-pustin, A., Wang, Y., and Tucker, J. C.:
855 Estimation of Terres- trial Global Gross Primary Production (GPP) with Satellite Data- Driven
856 Models and Eddy Covariance Flux Data, *Remote Sens.*, 10, 1346,
857 <https://doi.org/10.3390/rs10091346>, 2018.
- 858 Jung, M., Schwalm, C., Migliavacca, M., Walther, S., Camps-Valls, G., Koirala, S., et al. (2020). Scaling
859 carbon fluxes from eddy covariance sites to globe: synthesis and evaluation of the FLUXCOM
860 approach. *Biogeosciences*, 17(5), 1343–1365. <https://doi.org/10.5194/bg-17-1343-2020>
- 861 Kato, S., N. Loeb, F. G. Rose, D. R. Doelling, D. A. Rutan, T. E. Caldwell, L. Yu, and R. A. Weller
862 (2013), Surface irradiances consistent with CERES-derived top-of-atmosphere shortwave and
863 longwave irradiances. *J. Climate*, 26, 2719–2740, doi:10.1175/JCLI-D-12-00436.1.
- 864 Keppel-Aleks, G., and Washenfelder, R.A. 2016. "The effect of atmospheric sulfate reductions on diffuse
865 radiation and photosynthesis in the United States during 1995–2013." *Geophysical Research Letters*,
866 Vol. 43(No. 18): pp. 9984–9993. doi:10.1002/2016GL070052.
- 867 Kim, P. S., et al. (2015), Sources, seasonality, and trends of southeast US aerosol: an integrated analysis
868 of surface, aircraft, and satellite observations with the GEOS-Chem chemical transport model, *Atmos.*
869 *Chem. Phys.*, 15, 10411-10433, doi:10.5194/acp-15-10411-2015.
- 870 Koster, R. D., M. J. Suarez, A. Ducharme, M. Stieglitz, and P. Kumar, 2000: A catchment-based approach
871 to modeling land surface processes in a general circulation model: 1. Model structure. *J. Geophys.*
872 *Res.*, 105, 24 809–24 822, doi:10.1029/2000JD900327.
- 873 Koster, R. D., and G. K. Walker (2015), Interactive vegetation phenology, soil moisture, and monthly
874 temperature forecasts, *J. Hydrometeorol.*, 16, 1456–1465, doi:10.1175/JHM-D-14-0205.1.
- 875 Laurance, W.F. 1999. Gaia's lungs: Are rainforests inhaling Earth's excess carbon dioxide? *Natural*
876 *History* (April), p. 96.
- 877 Lawrence, D. M., Fisher, R. A., Koven, C. D., Oleson, K. W., Swenson, S. C., Bonan, G., et al. (2019).
878 The Community Land Model version 5: Description of new features, benchmarking, and impact of



- 879 forcing uncertainty. *Journal of Advances in Modeling Earth Systems*,
880 <https://doi.org/10.1029/2018MS001583>.
- 881 Min S. Lee, David Y. Hollinger, Trevor F. Keenan, Andrew P. Ouimette, Scott V. Ollinger, Andrew D.
882 Richardson, Model-based analysis of the impact of diffuse radiation on CO₂ exchange in a temperate
883 deciduous forest, *Agricultural and Forest Meteorology*, 249, 377–389,
884 <https://doi.org/10.1016/j.agrformet.2017.11.016>, 2018.
- 885 Letts, M. G., P.M. Lafleur, and N.T. Roulet, On the relationship between cloudiness and net ecosystem
886 carbon dioxide exchange in a peatland ecosystem *Ecoscience*, 12 (1) (2005), pp. 53–59.
- 887 Li, T. and Q. Yang, Advantages of diffuse light for horticultural production and perspectives for further
888 research. *Front Plant Sci.* 2015; 6: 704, published online 2015 Sep 4. doi: 10.3389/fpls.2015.00704.
- 889 Malavelle, F. F., Haywood, J. M., Mercado, L. M., Folberth, G. A., Bellouin, N., Sitch, S., and Artaxo, P.:
890 Studying the impact of biomass burning aerosol radiative and climate effects on the Amazon
891 rainforest productivity with an Earth system model, *Atmos. Chem. Phys.*, 19, 1301–1326,
892 <https://doi.org/10.5194/acp-19-1301-2019>, 2019.
- 893 Martin, S. T., M. O. Andreae, D. Althausen, P. Artaxo, H. Baars, S. Borrmann, Q. Chen, D. K. Farmer, A.
894 Guenther, S. S. Gunthe, J. L. Jimenez, T. Karl, K. Longo, A. Manzi, T. Müller, T. Pauliquevis, M. D.
895 Petters, A. J. Prenni, U. Pöschl, L. V. Rizzo, J. Schneider, J. N. Smith, E. Swietlicki, J. Tota, J. Wang,
896 A. Wiedensohler and S. R. Zorn (2010). "An overview of the Amazonian Aerosol Characterization
897 Experiment 2008 (AMAZE-08)." *Atmospheric Chemistry and Physics* 10(23): 11415–11438.
- 898 Mercado, L. M., N. Bellouin, S. Sitch, O. Boucher, C. Huntingford, M. Wild, and P. M. Cox (2009),
899 Impact of changes in diffuse radiation on the global land carbon sink, *Nature*, 458(7241), 1014–1017.
- 900 Molod, A., L. Takacs, M. Suarez, J. Bacmeister, I.-S. Song, and A. Eichmann, 2012. The GEOS-5
901 Atmospheric General Circulation Model: Mean Climate and Development from MERRA to Fortuna.
902 Technical Report Series on Global Modeling and Data Assimilation, 28, 2012
903 (<http://gmao.gsfc.nasa.gov/pubs/docs/Molod484.pdf>).
- 904 Molod, A., Takacs, L., Suarez, M., and Bacmeister, J.: Development of the GEOS-5 atmospheric general
905 circulation model: evolution from MERRA to MERRA2, *Geoscientific Model Development*, 8,
906 1339–1356, <https://doi.org/10.5194/gmd-8-1339-2015>, [https://www.geosci-model-](https://www.geosci-model-dev.net/8/1339/2015/)
907 [dev.net/8/1339/2015/](https://www.geosci-model-dev.net/8/1339/2015/), 2015.
- 908 Moreira, D. S., Longo, K. M., Freitas, S. R., Yamasoe, M. A., Mercado, L. M., Rosário, N. E., Gloor, E.,
909 Viana, R. S. M., Miller, J. B., Gatti, L. V., Wiedemann, K. T., Domingues, L. K. G., and Correia, C.
910 C. S.: Modeling the radiative effects of biomass burning aerosols on carbon fluxes in the Amazon
911 region, *Atmos. Chem. Phys.*, 17, 14785–14810, <https://doi.org/10.5194/acp-17-14785-2017>, 2017.
- 912 Murphy, D. M., Froyd, K. D., Bian, H., Brock, C. A., Dibb, J. E., DiGangi, J. P., Diskin, G., Dollner, M.,
913 Kupc, A., Scheuer, E. M., Schill, G. P., Weinzierl, B., Williamson, C. J., and Yu, P.: The distribution
914 of sea-salt aerosol in the global troposphere, *Atmos. Chem. Phys.*, 19, 4093–4104,
915 <https://doi.org/10.5194/acp-19-4093-2019>, Apr., 2019.
- 916 Myneni, R., Knyazikhin, Y., Park, T. (2015). MOD15A2H MODIS Leaf Area Index/FPAR 8-Day L4
917 Global 500m SIN Grid V006. NASA EOSDIS Land Processes DAAC.
918 <http://doi.org/10.5067/MODIS/MOD15A2H.006> (Terra) and
919 <http://doi.org/10.5067/MODIS/MYD15A2H.006> (Aqua).
- 920 Napstad, D., C. M. Stickler, B. Soares-Filho, and F. Merry, Interactions among Amazon land use, forests
921 and climate: prospects for a near-term forest tipping point, *Philos Trans R Soc Lond B Biol Sci.*;
922 363(1498): 1737–1746, doi: 10.1098/rstb.2007.0036, May 27, 2008.
- 923 Napstad DC, Stickler CM, Filho BS, Merry F. Interactions among Amazon land use, forests and climate:
924 prospects for a near-term forest tipping point. *Philos Trans R Soc Lond B Biol Sci.*
925 2008;363(1498):1737-1746. doi:10.1098/rstb.2007.0036.
- 926 Ng, N. L., S. C. Herndon, A. Trimborn, M. R. Canagaratna, P. L. Croteau, T. B. Onasch, D. Sueper, D. R.
927 Worsnop, Q. Zhang, Y. L. Sun and J. T. Jayne (2011). "An Aerosol Chemical Speciation Monitor
928 (ACSM) for Routine Monitoring of the Composition and Mass Concentrations of Ambient Aerosol."
929 *Aerosol Science and Technology* 45(7): 780–794.



- 930 Niyogi, D., et al. (2004), Direct observations of the effects of aerosol loading on net ecosystem CO₂
931 exchanges over different landscapes, *Geophys. Res. Lett.*, 31, L20506, doi:10.1029/2004GL020915.
- 932 Oliveira, P. H. F., P. Artaxo, C. Pires, S. De Lucca, A. Procopio, B. Holben, J. Schafer, L. F. Cardoso, S.
933 C. Wofsy, and H. R. Rocha (2007), The effects of biomass burning aerosols and clouds on the CO₂
934 flux in Amazonia, *Tellus, Ser. B*, 59(3), 338–349.
- 935 Oleson, K. W., and Coauthors, 2010: Technical description of version 4.0 of the Community Land Model
936 (CLM). NCAR Tech. Note NCAR/TN-478+STR, 257 pp.
- 937 Oleson, K. W., Lawrence, D. M., Bonan, G. B., Drewniak, B., Huang, M., Koven, C. D., Levis, S., Li,
938 F., Riley, W. J., Subin, Z. M., Swenson, S. C., Thornton, P. E., Bozbiyik, A., Fisher, R., Heald, C.
939 L., Kluzek, E., Lamarque, J.-F., Lawrence, P. J., Leung, L. R., Lipscomb, W., Muszala, S., Ricciuto,
940 D. M., Sacks, W., Sun, Y., Tang, J., & Yang, Z.-L. (2013). Technical description of version 4.5 of
941 the Community Land Model (CLM), NCAR Tech. Note NCAR/TN-503+STR. National Center for
942 Atmospheric Research, Boulder, Colorado, 420 pp.
- 943 O'Sullivan, M., A. Rap, C. L. Reddington, D. V. Spracklen, M. Gloor, W. Buermann, Small global
944 effect on terrestrial net primary production due to increased fossil fuel aerosol emissions
945 from East Asia since the turn of the century, *Geophys Res Lett.* 2016 Aug 16; 43(15): 8060–
946 8067. doi: 10.1002/2016GL068965, 2016.
- 947 Rap, A., Spracklen, D. V., Mercado, L., Reddington, C. L., Haywood, J. M., Ellis, R. J., Phillips, O. L.,
948 Artaxo, P., Bonal, D., Restrepo Coupe, N., and Butt, N.: Fires increase amazon forest productivity
949 through increases in diffuse radiation, *Geophys. Res. Lett.*, 42, 4654–4662
950 doi:10.1002/2015GL063719, 2015.
- 951 Rap, A., Scott, C.E., Reddington, C.L. et al. Enhanced global primary production by biogenic aerosol via
952 diffuse radiation fertilization. *Nature Geosci* 11, 640–644 (2018). [https://doi.org/10.1038/s41561-](https://doi.org/10.1038/s41561-018-0208-3)
953 [018-0208-3](https://doi.org/10.1038/s41561-018-0208-3).
- 954 Randles, C. A., Kinne, S., Myhre, G., Schulz, M., Stier, P., Fischer, J., Doppler, L., Highwood, E., Ryder,
955 C., Harris, B., Huttunen, J., Ma, Y., Pinker, R. T., Mayer, B., Neubauer, D., Hitzenberger, R.,
956 Oreopoulos, L., Lee, D., Pitari, G., Di Genova, G., Quaas, J., Rose, F. G., Kato, S., Rumbold, S. T.,
957 Vardavas, I., Hatzianastassiou, N., Matsoukas, C., Yu, H., Zhang, F., Zhang, H., and Lu, P.:
958 Intercomparison of shortwave radiative transfer schemes in global aerosol modeling: results from the
959 AeroCom Radiative Transfer Experiment, *Atmos. Chem. Phys.*, 13, 2347–2379,
960 <https://doi.org/10.5194/acp-13-2347-2013>, 2013.
- 961 Randles, C. A., da Silva, A. M., Buchard, V., Colarco, P. R., Darmenov, A., Govindaraju, R., et al.
962 (2017). The MERRA-2 Aerosol Reanalysis, 1980 Onward. Part I: System Description and Data
963 Assimilation Evaluation. *Journal of Climate*. <https://doi.org/10.1175/JCLI-D-16-0609.1>
- 964 Rienecker, M. M., M. J. Suarez, R. Gelaro, R. Todling, J. Bacmeister, E. Liu, M. G. Bosilovich, S. D.
965 Schubert, L. Takacs, G.-K. Kim, S. Bloom, J. Chen, D. Collins, A. Conaty, A. da Silva, W. Gu, J.
966 Joiner, R. D. Koster, R. Lucchesi, A. Molod, T. Owens, S. Pawson, P. Pegion, C. R. Redder, R.
967 Reichle, F. R. Robertson, A. G. Ruddick, M. Sienkiewicz, J. Woollen, MERRA - NASA's Modern-
968 Era Retrospective Analysis for Research and Applications. *J. Climate*, 24, 3624–3648, 2011.
- 969 Roderick, M. L., G. D. Farquhar, S. L. Berry, and I. R. Noble (2001), On the direct effect of clouds and
970 atmospheric particles on the productivity and structure of vegetation, *Oecologia*, 129(1), 21–30.
- 971 Saatchi S, Asefi-Najafabady S, Malhi Y, Arag-ao LEOC, Anderson LO, Myneni RB, Nemani R (2013)
972 Persistent effects of a severe drought on Amazonian forest canopy. *Proceedings of the National*
973 *Academy of Sciences of the United States of America*, 110, 565–570.
- 974 Shilling, J. E., M. S. Pekour, E. C. Fortner, P. Artaxo, S. de Sá, J. M. Hubbe, K. M. Longo, L. A. T.
975 Machado, S. T. Martin, S. R. Springston, J. Tomlinson and J. Wang (2018). "Aircraft Observations of
976 Aerosol in the Manaus Urban Plume and Surrounding Tropical Forest during GoAmazon 2014/15."
977 *Atmos. Chem. Phys. Discuss.* 2018: 1-37.



- 978 Sporre, M. K., Blichner, S. M., Karset, I. H. H., Makkonen, R., and Berntsen, T. K.: BVOC–aerosol–
979 climate feedbacks investigated using NorESM, *Atmos. Chem. Phys.*, 19, 4763–
980 4782, <https://doi.org/10.5194/acp-19-4763-2019>, 2019.
- 981 Thornton, P. E., & Zimmermann, N. E. (2007). An improved canopy integration scheme for a land
982 surface model with prognostic canopy structure. *Journal Of Climate*, 20, 3902-3923.
983 doi:10.1175/JCLI4222.1.
- 984 University of Oklahoma. "Dry season increase in photosynthesis in Amazon rain forest." *ScienceDaily*.
985 *ScienceDaily*, 22 October 2019. <www.sciencedaily.com/releases/2019/10/191022092804.htm>
- 986 Wang, X., Wu, J., Chen, M., Xu, X., Wang, Z., Wang, B., Wang, C., Piao, S., Lin, W., & Miao,
987 G. (2018). Field evidences for the positive effects of aerosols on tree growth. *Global Change*
988 *Biology*, 24, 4983–4992. <https://doi.org/10.1111/gcb.14339>.
- 989 Wild, O., X. Zhu, and M. Prather, Fast-J: Accurate simulation of in- and below-cloud photolysis in
990 tropospheric chemical models, *J. Atmos. Chem.* 37, 245-282, 2000.
- 991 Xi, X., and I. N. Sokolik, 2012: Impact of Asian dust aerosol and surface albedo on photosynthetically
992 active radiation and surface radiative balance in dryland ecosystems. *Advances in Meteorology*, 2012,
993 Article ID 276207, doi: 10.1155/2012/276207.
- 994 Yan, X., W. Z. Shi, W. J. Zhao, et al., 2014: Impact of aerosols and atmospheric particles on plant leaf
995 proteins. *Atmos. Environ.*, 88, 115–122, doi: <https://doi.org/10.1016/j.atmosenv.2014.01.044>.
- 996 Zhou, Yanlian; Xiaocui Wu; Weimin Ju; Leiming Zhang; Zhi Chen; Wei He; Yibo Liu; Yang Shen,
997 Modeling the Effects of Global and Diffuse Radiation on Terrestrial Gross Primary Productivity in
998 China Based on a Two-Leaf Light Use Efficiency Model, *Remote Sens.* 12(20),
999 3355; <https://doi.org/10.3390/rs12203355>, 2020.